# TE Modes in Liquid Crystal Optical Fibers Embedded with Conducting Tape Helix Structure

Masih Ghasemi and P. K. Choudhury
*Institute of Microengineering and Nanoelectronics, Universiti Kebangsaan Malaysia, U.K.M. Bangi, 43600, Malaysia*

Keywords: Liquid Crystal Fibers, Complex Optical Microstructures, Electromagnetic Waves.

Abstract: The transverse electric (TE) behaviour of light in a doubly-clad cylindrical optical fiber loaded with radially anisotropic liquid crystal material at the outermost cladding is investigated. Moreover, this situation is studied when a conducting tape helix structure is introduced at the boundary of the isotropic dielectric core and the inner dielectric clad of the fiber. The outer clad is considered to be made of anisotropic nematic liquid crystal (NLC). Using Maxwell's electromagnetic field equations, confinement plots are obtained for the transmitted power in each scenario, under the situation of varying core dimension, and compared. Results confirm the achievement of better confinement in the liquid crystal layer of the conducting tape helix loaded fiber, which can even be tailored by using different angle of helix pitch.



## 1 INTRODUCTION

Nonlinear properties of liquid crystals (LCs) have been utilized in variety of applications in optics industries. For instance, the latest research illustrates the impact of temperature on the optical harmonic generation in fiber-coupled nematic LCs (Trashkeev *et al.*, 2014). Other report shows that LC fiber array would confine transmission of high energy laser pulses, which can be exploited as protector for downstream sensors (Khoo *et al.*, 1996). The literature on LC based waveguides proved potentials of research concealed behind the dispersion property of radial anisotropy orientation of LC material (Ioannidis *et al.*, 1991).

Apart from the aforementioned applications, LCs are greatly useful for devising various forms of sensing and field coupling needs that include optical sensors as well. For example, such materials become indispensable in fabricating lasers (Dolgaleva *et al.*, 2009), polarimetric sensors (Wolinski *et al.*, 2001), dispersion compensators (Akbulut, 2006), imaging systems (Gebhart *et al.*, 2005), electric field and temperature sensors (Wolinski *et al.*, 2006), photonic crystal based guides (Wolinski *et al.*, 2005), optical filters (Stratis *et al.*, 2001), integrated optic devices (d'Alessandro, 2004) etc. Within the context, optical fibers based on liquid crystals can be given a serious thought, and the sensing applications of such LC fibers have been investigated before (Choudhury, 2014). It has been reported earlier that tapering the fiber cross-section greatly enhances the optical sensing capability of LC based fibers (Choudhury *et al.*, 2011).

Amalgamation of material and geometrical properties could be the possible way to govern the lightwave propagation in waveguide technologies (Choudhury *et al.*, 2004; Ghasemi *et al.*, 2014). Apart from the LC material, perfectly conducting twisted clad fibers have also been reported as useful complex mediums wherein the pitch angle of conducting sheath or tape helices impose great control over the propagation characteristics of electromagnetic waves (Ghasemi *et al.*, 2014).

In the present paper, we deal with a three-layer optical fiber with the outermost region being coated with radially anisotropic LC material, and the inner dielectric core-clad interface is loaded with conducting tape helix structure. It must be remembered that the thickness of conducting tape remains infinitesimally small, which makes one to assume this parameter as almost vanishing. As such, the perpendicular component of surface current over the tape may be ignored, as compared to the parallel one. With the assumption of the availability of the flow of current over the surface of tape, recent report emphasized that the LC layer is more prone to confine the transmission of power for the lowest zero-order hybrid mode (Ghasemi *et al.*, 2014). In

Ghasemi M. and Choudhury P..
TE Modes in Liquid Crystal Optical Fibers Embedded with Conducting Tape Helix Structure.
DOI: 10.5220/0005319800610066
In *Proceedings of the 3rd International Conference on Photonics, Optics and Laser Technology* (PHOTOPTICS-2015), pages 61-66
ISBN: 978-989-758-092-5

the present work, we emphasize on the confinement due to transverse electric (TE) modes under varying tape helix pitch angle. Results reveal that small changes in the angle of pitch bring in considerable shifts in the characteristics of power transmission properties. The $TE_{01}$ mode with lower propagation constants transmits lower amount of power, and the fractional power increases with the increase in propagation constant in LC layer of fiber structure under consideration. The results are also compared with the situation when the tape helix structure is eliminated, in order to investigate the effect of the presence of conducting tape helical windings.

## 2 THEORY

Figures 1a and 1b, respectively, illustrate the schematics of LC optical fibers with and without conducting tape helix loadings. In the case of fig. 1a, $\psi$ represents the helix pitch angle, which may assume values between 0° and 90°. For the sake of simplicity, the LC layer is considered to be infinitely extended in the radial direction, whereas the inner isotropic dielectric core and the clad sections have the radius values as $a$ and $b$, respectively. The refractive index (RI) of the core and the inner clad regions are taken to be $n_{co}$ and $n_{ic}$, respectively. Owing to the ordinary and the extraordinary orientations of the outermost LC layer, we consider $n_o$ and $n_e$ as the respective RI values belonging to each orientation. Numerically, the RI distribution profile may be written as $n_e > n_{co} > n_{cl} > n_o$.

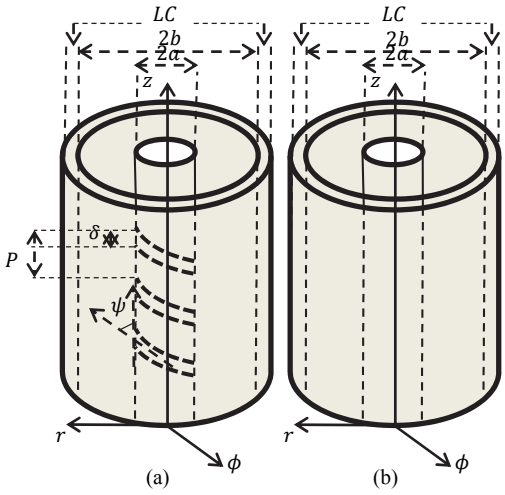


Figure 1: Schematic diagram of the LC fiber embedded with conducting tape helix (a) and without tape helix (b) structure.

The cylindrical polar coordinate system $(r, \phi, z)$ is used for the analysis of fibers with conducting tape helix loadings. We consider that the time $t$- and axis $z$-harmonic electromagnetic waves propagate along the $z$-direction. Considering fig. 1a, the parameters $\psi$, $\delta$ and $P$, respectively, represent the pitch angle of conducting tape helix, width of the conducting tape and the distance between two successive tape helical windings. However, it must be noted that $P$ and $\psi$ are related through

$$\psi = \arctan(P/2\pi a) \tag{1}$$

Equation (1) indicates that the helix pitch angle essentially depends on the fiber core dimension. As such, in the present investigation, computations are made for different values of core diameter, which provide particular values of pitch angle.

It must be remembered that, while investigating the $TE_{01}$ mode in the fiber structure, the only available fundamental electric fields component is $e_\phi$, which is independent of the coordinate $\phi$; the other components of field vanish. As such, we consider $\partial e_\phi/\partial r = 0$, and the solutions of the coupled differential equations contain Bessel and the modified Bessel functions (Snyder *et al.*, 1983).

$$G_{(l,s)}(r) = \begin{cases} l = 1, s = 0: J_{n-1}(Ur) & 0 < r < a \\ l = 2: \begin{cases} s = 0, K_{n-1}(Wr) \\ s = 1, I_{n-1}(Wr) \end{cases} & b < r < a \\ l = 3: H_{n-1}^{(2)}(Vr) & b < r < \infty \end{cases} \tag{2}$$

Equation (2) is written in symbolic form where $l$ the number of layer that corresponds to each region of fiber and $s$ represents subpart of the combined Bessel function within each layer. More explicitly, $G_{(1,0)}$ is Bessel function of the first kind in the first layer, $G_{(2,0)}$ and $G_{(2,1)}$ are the modified Bessel functions in the second layer, and $G_{(3,0)}$ is Hankel function of the second kind in the third layer of the LC fiber. Furthermore, the quantities $U$, $W$ and $V$ related to the core, the inner clad and the outer clad parameters, respectively, are defined as

$$U = \sqrt{(n_{co}^2 k^2 - \beta^2)} \tag{3}$$

$$W = \sqrt{(\beta^2 - n_{cl}^2 k^2)} \tag{4}$$

$$V = \sqrt{(\beta^2 - n_o^2 k^2)} \tag{5}$$

Upon substituting the above eq. (2) in Maxwell's equations, we finally obtain the following axial, radial and azimuthal components of electromagnetic field in the different fiber sections:

$$h_{z_1} = -\frac{A}{j\mu\omega r}\left\{G_{(1,0)}(r) + r\frac{d}{dr}G_{(1,0)}(r)\right\} \tag{6}$$

$$h_{r_1} = -\frac{A}{j\beta}\left[\frac{1}{j\mu\omega r^2}\left\{G_{(1,0)}(r) + r\frac{d}{dr}G_{(1,0)}(r)\right\} + \frac{1}{j\mu\omega r}\left\{2\frac{d}{dr}G_{(1,0)}(r) + r\frac{d^2}{dr^2}G_{(1,0)}(r)\right\} + j\omega\varepsilon_{(1,0)}G_{(1,0)}(r)\right] \quad (7)$$

$$e_{\varphi_1} = AG_{(1,0)}(r) \quad (8)$$

$$h_{z_2} = -\frac{B}{j\mu\omega r}\left\{G_{(2,0)}(r) + r\frac{d}{dr}G_{(2,0)}(r)\right\} - \frac{C}{j\mu\omega r}\left\{G_{(2,1)}(r) + r\frac{d}{dr}G_{(2,1)}(r)\right\} \quad (9)$$

$$h_{r_2} = -\frac{B}{j\beta}\left[\frac{1}{j\mu\omega r^2}\left\{G_{(2,0)}(r) + r\frac{d}{dr}G_{(2,0)}(r)\right\} + \frac{1}{j\mu\omega r}\left\{2\frac{d}{dr}G_{(2,0)}(r) + r\frac{d^2}{dr^2}G_{(2,0)}(r)\right\} + j\omega\varepsilon_{(2,0)}G_{(2,0)}(r)\right] - \frac{C}{j\beta}\left[\frac{1}{j\mu\omega r^2}\left\{G_{(2,1)}(r) + r\frac{d}{dr}G_{(2,1)}(r)\right\} + \frac{1}{j\mu\omega r}\left\{2\frac{d}{dr}G_{(2,1)}(r) + r\frac{d^2}{dr^2}G_{(2,1)}(r)\right\} + j\omega\varepsilon_{(2,1)}G_{(2,1)}(r)\right] \quad (10)$$

$$e_{\varphi_2} = BG_{(2,0)}(r) + CG_{(2,1)}(r) \quad (11)$$

$$h_{z_3} = -\frac{D}{j\mu\omega r}\left\{G_{(3,0)}(r) + r\frac{d}{dr}G_{(3,0)}(r)\right\} \quad (12)$$

$$h_{r_3} = -\frac{D}{j\beta}\left[\frac{1}{j\mu\omega r^2}\left\{G_{(3,0)}(r) + r\frac{d}{dr}G_{(3,0)}(r)\right\} + \frac{1}{j\mu\omega r}\left\{2\frac{d}{dr}G_{(3,0)}(r) + r\frac{d^2}{dr^2}G_{(3,0)}(r)\right\} + j\omega\varepsilon_{(3,0)}G_{(3,0)}(r)\right] \quad (13)$$

$$e_{\varphi_3} = DG_{(3,0)}(r) \quad (14)$$

In the above equations, $A$, $B$, $C$ and $D$ are the (unknown) arbitrary constants, which are to be determined by the use of suitable boundary conditions (Ghasemi *et al.*, 2014). The relevant analytical treatment ultimately yields the values of these constants as

$$A = \varrho_0\alpha_1\alpha_2 \quad (15)$$

$$B = \varrho_0\alpha_3\alpha_2 \quad (16)$$

$$C = \varrho_0\alpha_1 \quad (17)$$

$$D = \varrho_0\alpha_1\alpha_4 \quad (18)$$

where $\varrho_0$ is the total current density over surface of tape helix, as obtained by using the tangential components of magnetic field in the core and the inner clad regions of fiber. Corresponding to the situation of $TE_{01}$ mode, $\varrho_0$ would assume the form

$$\varrho_0 = \frac{\varsigma_0}{2P\cos(\psi)}e^{\frac{j(\beta_0\cos^2\psi)\delta}{2}}J_0(\beta_0\cos^2\psi)\delta \quad (19)$$

Further, the other symbols used in eqs. (15)–(18) have meanings as follows:

$$\alpha_1 = \frac{1}{\sin\psi\left(\alpha_6 + \alpha_4\alpha_5\frac{\chi_7^b}{\chi_3^b} - \frac{\chi_4^b}{\chi_3^b}\right)} \quad (20)$$

$$\alpha_2 = \frac{\alpha_5\chi_3^a + \chi_4^a}{\chi_1^a} \quad (21)$$

$$\alpha_3 = \frac{\alpha_4\chi_7^b - \chi_4^b}{\chi_3^b} \quad (22)$$

$$\alpha_4 = \frac{\frac{\chi_4^b}{\chi_3^b}\chi_5^b - \chi_6^b}{\frac{\chi_7^b}{\chi_3^b}\chi_5^b - \chi_8^b} \quad (23)$$

$$\alpha_5 = \frac{\chi_3^a}{\chi_1^a}\chi_2^a - \chi_5^a \quad (24)$$

$$\alpha_6 = \frac{\chi_4^a}{\chi_1^a}\chi_2^a + \chi_6^a \quad (25)$$

with

$$\chi_1^a = G_{(1,0)}(a) \quad (26)$$

$$\chi_2^a = -\frac{1}{j\mu\omega r}\left\{G_{(1,0)}(a) + r\frac{d}{dr}G_{(1,0)}(a)\right\} \quad (27)$$

$$\chi_3^a = G_{(2,0)}(a) \quad (28)$$

$$\chi_4^a = G_{(2,1)}(a) \quad (29)$$

$$\chi_5^a = -\frac{1}{j\mu\omega r}\left\{G_{(2,0)}(a) + r\frac{d}{dr}G_{(2,0)}(a)\right\} \quad (30)$$

$$\chi_6^a = -\frac{1}{j\mu\omega r}\left\{G_{(2,1)}(a) + r\frac{d}{dr}G_{(2,1)}(a)\right\} \quad (31)$$

$$\chi_3^b = G_{(2,0)}(b) \quad (32)$$

$$\chi_4^b = G_{(2,1)}(b) \quad (33)$$

$$\chi_5^b = -\frac{1}{j\mu\omega r}\left\{G_{(2,0)}(b) + r\frac{d}{dr}G_{(2,0)}(b)\right\} \quad (34)$$

$$\chi_6^b = -\frac{1}{j\mu\omega r}\left\{G_{(2,1)}(b) + r\frac{d}{dr}G_{(2,1)}(b)\right\} \quad (35)$$

$$\chi_7^b = G_{(3,0)}(b) \quad (36)$$

$$\chi_8^b = -\frac{1}{j\mu\omega r}\left\{G_{(3,1)}(b) + r\frac{d}{dr}G_{(3,1)}(b)\right\} \quad (37)$$

In the case of fiber with the loading of conducting tape helix (fig. 1a), we consider that the flow of current takes place over the surface of tape. However, in the case of fig. 1b, fields remain continuous at each boundary, and power confinements are derived from the continuity conditions. The elimination of conducting tape will essentially cause the expressions of electric and magnetic components to have different set unknown constants, viz. $A'$, $B'$, $C'$ and $D'$. Thus, we can have the field components in this case as

$$h'_{z_1} = -\frac{A'}{j\mu\omega r}\left\{G_{(1,0)}(r) + r\frac{d}{dr}G_{(1,0)}(r)\right\} \quad (38)$$

$$h'_{r_1} = -\frac{A'}{j\beta}\left[\frac{1}{j\mu\omega r^2}\left\{G_{(1,0)}(r) + r\frac{d}{dr}G_{(1,0)}(r)\right\} + \frac{1}{j\mu\omega r}\left\{2\frac{d}{dr}G_{(1,0)}(r) + r\frac{d^2}{dr^2}G_{(1,0)}(r)\right\} + j\omega\varepsilon_{(1,0)}G_{(1,0)}(r)\right] \quad (39)$$

$$e'_{\varphi_1} = A'G_{(1,0)}(r) \quad (40)$$

$$h'_{z_2} = -\frac{B'}{j\mu\omega r}\left\{G_{(2,0)}(r) + r\frac{d}{dr}G_{(2,0)}(r)\right\} + -\frac{C}{j\mu\omega r}\left\{G_{(2,1)}(r) + r\frac{d}{dr}G_{(2,1)}(r)\right\} \quad (41)$$

$$h'_{r_2} = -\frac{B'}{j\beta}\left[\frac{1}{j\mu\omega r^2}\left\{G_{(2,0)}(r) + r\frac{d}{dr}G_{(2,0)}(r)\right\} + \frac{1}{j\mu\omega r}\left\{2\frac{d}{dr}G_{(2,0)}(r) + r\frac{d^2}{dr^2}G_{(2,0)}(r)\right\} + j\omega\varepsilon_{(2,0)}G_{(2,0)}(r)\right] - \frac{C}{j\beta}\left[\frac{1}{j\mu\omega r^2}\left\{G_{(2,1)}(r) + r\frac{d}{dr}G_{(2,1)}(r)\right\} + \frac{1}{j\mu\omega r}\left\{2\frac{d}{dr}G_{(2,1)}(r) + r\frac{d^2}{dr^2}G_{(2,1)}(r)\right\} + j\omega\varepsilon_{(2,1)}G_{(2,1)}(r)\right] \quad (42)$$

$$e'_{\varphi_2} = B'G_{(2,0)}(r) + C'G_{(2,1)}(r) \quad (43)$$

$$h'_{z_3} = -\frac{D'}{j\mu\omega r}\left\{G_{(3,0)}(r) + r\frac{d}{dr}G_{(3,0)}(r)\right\} \quad (44)$$

$$h'_{r_3} = -\frac{D'}{j\beta}\left[\frac{1}{j\mu\omega r^2}\left\{G_{(3,0)}(r) + r\frac{d}{dr}G_{(3,0)}(r)\right\} + \frac{1}{j\mu\omega r}\left\{2\frac{d}{dr}G_{(3,0)}(r) + r\frac{d^2}{dr^2}G_{(3,0)}(r)\right\} + j\omega\varepsilon_{(3,0)}G_{(3,0)}(r)\right] \quad (45)$$

$$e'_{\varphi_3} = D'G_{(3,0)}(r) \quad (46)$$

Equations (38)–(46) can be exploited to implement the continuity conditions of fields corresponding to the non-helix kind of LC fiber. Further, eqs. (26)–(37) can be utilized in order to extract the expressions for the unknown constants corresponding to the $TE_{01}$ mode excitation. Finally, the unknown constants $A'$ $B'$ and $C'$ will assume the forms, in terms of $D'$, as follows:

$$A' = \frac{\left(\frac{\zeta_1}{\zeta_2}\chi_1^a + \frac{1}{\zeta_2}\chi_4^a\right)}{\chi_1^a}D' \quad (47)$$

$$B' = \frac{\zeta_1}{\zeta_2}D' \quad (48)$$

$$C' = \frac{1}{\zeta_2}D' \quad (49)$$

with

$$\zeta_1 = \frac{\left(\frac{\chi_6^a}{\chi_2^a} - \frac{\chi_4^a}{\chi_1^a}\right)}{\left(\frac{\chi_3^a}{\chi_1^a} - \frac{\chi_5^a}{\chi_2^a}\right)} \quad (50)$$

$$\zeta_2 = \frac{\left(\frac{\chi_4^b}{\chi_3^b} - \frac{\chi_6^b}{\chi_5^b}\right)}{\left(\frac{\chi_7^b}{\chi_3^b} - \frac{\chi_8^b}{\chi_5^a}\right)} \quad (51)$$

Finally, in order to compute the propagation of power through the LC fiber structures of fig. 1, we use eqs. (15)–(18) corresponding to the case of conducting tape helix based fiber (fig. 1a), whereas eqs. (47)–(49) for the fiber without the existence of tape helix structure (fig. 1b). Furthermore, by the use of electromagnetic field equations corresponding to the case of particular fiber, the expressions for the confinement of power in the different fiber regions for the respective LC fiber structure can be deduced.

# 3 RESULTS AND DISCUSSION

We now make attempts to evaluate the confinement of power in the fiber structures of fig. 1 due to the transmission of the $TE_{01}$ mode. At this point, this must be remembered that, as stated above, the entire mathematical treatment is not incorporated into the text, in order to avoid the length of the manuscript.

For the computational purpose, we assume the RI values of the core and the inner clad sections as $n_{co} = 1.462$ and $n_{cl} = 1.458$, respectively, while in the LC layer we take the nematic liquid crystal as BDH mixture 14616 having the respective ordinary and the extra ordinary RI values as $n_o = 1.457$ and $n_e = 1.5037$. The wavelength of operation is taken as 633 nm. Further, it must be remembered that, in the evaluation of power, the distance $P$ between two consecutive tape helix windings is governed by the following expression:

$$P = (\lambda/2n_{co}) \times (n_{co} + n_{cl})/n_{co}n_{cl} \quad (52)$$

Figures 2a, 2b and 2c illustrate the plots of the propagation of power in the core, the inner clad and the outer clad sections, respectively, under the situation when the LC fiber is assumed to have a loading of conducting tape helix with specific orientation. For this purpose, we consider five different values of fiber core dimension through setting the value of $a$ as 5 μm, 15 μm, 30 μm, 50 μm and 70 μm. Also, the inner clad size is taken to be fixed with $b$ as 150 μm, while the outermost LC clad is extended to infinity. Furthermore, we consider that $\delta$, the width of the tape, is 10 times smaller than the pitch $P$ formed due to the gap between two successive windings of conducting tape helix. Since the pitch of helix has inverse relationship with the core size, the lowest value of pitch corresponds to the largest core size. The aforementioned values of $a$ give the respective values of helix pitch angles as 0.79°, 0.26°, 0.13°, 0.08° and 0.06°. In figs. 2, plots of confinements are illustrated corresponding to these specific values of $\psi$ that essentially represent varying orientation of conducting tape helix.

We observe from fig. 2a that the confinement due to the $TE_{01}$ mode remains very small in the core section, particularly for the higher values of propagation constant. Corresponding to all the values of fiber core dimension, it gradually decreases with the increase in $\beta$-values. In the inner

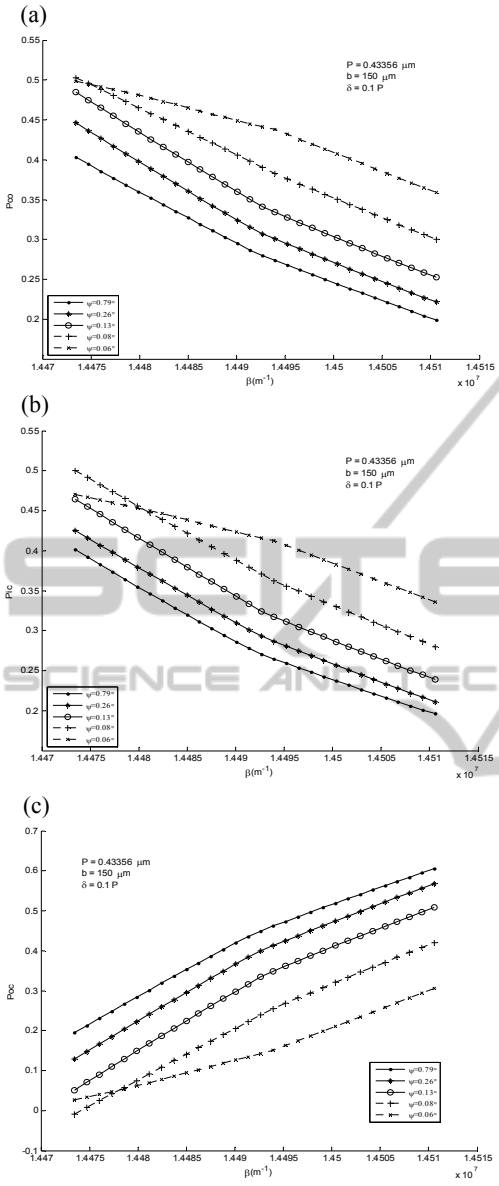


Figure 2: $TE_{01}$ mode power confinement patterns in the fiber (a) core, (b) inner clad, and (c) LC outer clad in the case of conducting tape helix loaded LC fiber.

clad section too, the behaviour of power distribution remains almost similar (fig. 2b). Figure 2c illustrates that, for higher $\beta$-values, the confinement is markedly increased, and remains the maximum corresponding to the maximum value of helix pitch angle. For $\psi = 0.79°$, we find from fig. 2c that the confinement varies between 20%–65% over the allowed values of propagation constant.

In order to have a comparative look, investigations are made of the LC fiber without the loading of the conducting tape helix windings, and the corresponding plots are shown in fig. 3. In this set of figures, we observe that, in every section of fiber structure, confinement due to the $TE_{01}$ mode becomes smaller, as compared to the situation of fiber with tape helix (fig. 2).

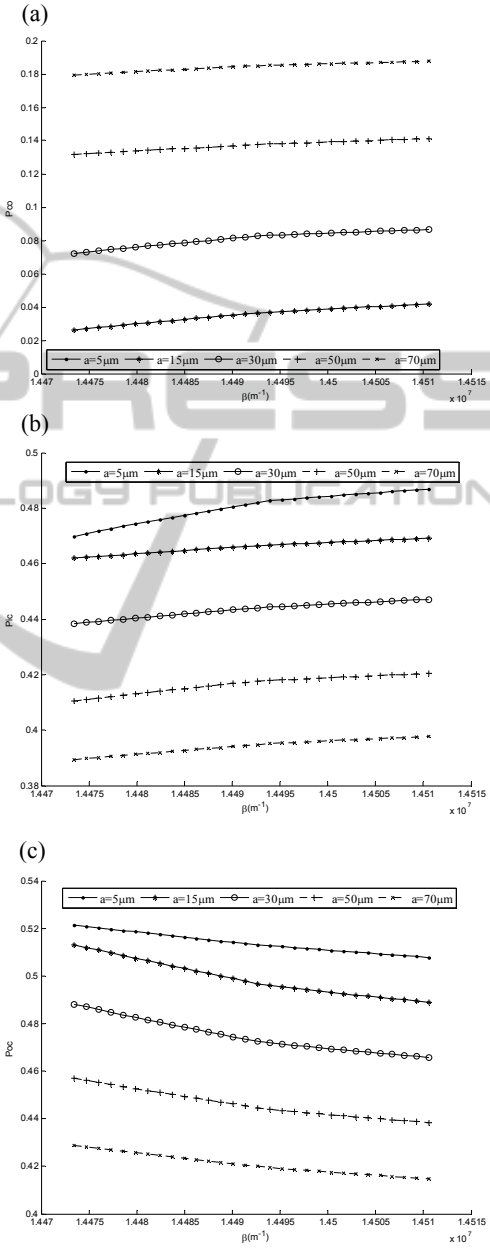


Figure 3: $TE_{01}$ mode power confinement patterns in the fiber (a) core, (b) inner clad, and (c) LC outer clad in the case of LC fiber.

Our prime interest remains on the way to increase the confinement of power in the outermost section of fiber. We, therefore, observe that the fiber

embedded with conducting tape helix structure remains capable to sustain more amount of power in the outermost liquid crystal section. This essentially makes the structure possibly more efficient for its usages like the integrated optic devices for field coupling and/or in the area of optical sensing.

## 4 CONCLUSIONS

From the foregoing analyses, it can be inferred that the LC fiber structure loaded with conducting tape helix windings would be more useful for applications in optics industry. This is primarily due to the reason that the outermost liquid crystal region becomes more prone to confine higher amount of power to be used particularly for the evanescent field based optical applications (e.g. sensing or coupling of electromagnetic fields). These conclusive remarks are drawn based on comparing the results obtained for ordinary LC clad fibers with radially anisotropic liquid crystal materials.

## ACKNOWLEDGEMENTS

The authors are thankful to the Ministry of Higher Education (Malaysia) for granting the financial support to the work Also, they are thankful to Professors B.Y. Majlis and S. Shaari for constant encouragement and help.

## REFERENCES

Trashkeev, S. I., Nyushkov, B. N., 2014. Thermal enhancement of optical harmonic generation in a fiber-coupled nematic liquid crystal. *Laser Optics 2014 – IEEE International Conference*, pp. 1–1.

Khoo, I. C., Wood, M., Guenther, B. D., 1996. Nonlinear liquid crystal optical fiber array for all-optical switching/limiting. In *LEOS 96 – IEEE Lasers and Electro-Optics Society Annual Meeting*, vol. 2, pp. 211–212.

Ioannidis, Z. K., Giles, I. P., Bowry, C., 1991. All-fiber optic intensity modulators using liquid crystals, *Appl. Opt.*, vol. 30, pp. 328–333.

Dolgaleva, K., Wei, S. K. H., Lukishova, S. G., Chen, S.H., Schwertz, K., Boyd, R.W., 2009. Enhanced laser performance of cholesteric liquid crystals doped with oligofluorene dye. *J. Opt. Soc. Am. B*, vol. 25, pp. 1496–1504.

Wolinski, T. R., Szymanska, A., 2001. Polarimetric optical fibres with elliptical liquid-crystal core. *Meas. Sci. Technol.*, vol. 12, pp. 948−951.

Akbulut, M., 2006. Broadband all-order polarization mode dispersion compensation using liquid-crystal modulator arrays. *J. Lightwave Technol.*, vol. 24, pp. 251−261.

Gebhart, S. C., Stokes, D. L., Vo-Dinh, T., Mahadevan-Jansen, A., 2005. Instrumentation considerations in spectral imaging for tissue demarcation: comparing three methods of spectral resolution. *Proc. SPIE*, vol. 5694, pp. 41−52.

Wolinski, T. R., Szaniawska, K., Ertman, S., Lesiak, P., Domanski, A.W., Dabrowski, R., Nowinowski-Kruszelnicki, E., Wojcik, J., 2006. Influence of temperature and electrical fields on propagation properties of photonic liquid-crystal fibres. *Meas. Sci. Technol.*, vol. 17, pp. 985–991.

Wolinski, T. R., Szaniawska, K., Bondarczuk, K., Lesiak, P., Domanski, A. W., Dabrowski, R., Nowinowski-Kruszelnicki, E., Wojcik, J., 2005. Propagation properties of photonic crystal fibers filled with nematic liquid crystals. *Opto-Electron. Rev.*, vol. 13, pp. 59–64.

Stratis, D. N., Eland, K. L., Carter, J. C., Tomlinson, S. J., Angel, S.M., 2001. Comparison of acousto-optic and liquid crystal tunable filters for laser-induced breakdown spectroscopy. *Appl. Spectroscop.*, vol. 55, pp. 999−1004.

d'Alessandro, A., Asquini, R., Gizzi, C., Bellini, B., Beccherelli, R., 2004. Integrated optic devices using liquid crystals: design and fabrication issues. *Proc. SPIE*, vol. 5518, pp. 123−135.

Choudhury, P. K., 2013. Liquid crystal optical fibers for sensing applications. *Proc. SPIE*, vol. 8818, pp. 88180E-1–88180E-10.

Choudhury, P. K., Soon, W. K., 2011. On the transmission by liquid crystal tapered optical fibers. *Optik*, vol. 122, pp. 1061−1068 (2011).

Choudhury, P. K., Yoshino, T., 2004. TE and TM modes power transmission through liquid crystal optical fibers. *Optik*, vol. 115, pp. 49−56.

Ghasemi, M., Choudhury, P. K., 2014. Propagation through complex structured liquid crystal optical fibers. *J. Nanophoton.*, vol. 8, pp. 083997-1–083997-13.

Ghasemi, M., Choudhury, P. K., 2014. Waves in tape helix loaded liquid crystal optical fiber. *Proc. SPIE*, vol. 9172, pp. 91720G-1–91720G-8.

Snyder, A. W., Rühl, F., 1983. Single-mode, single-polarization fibers made of birefringent material. *J. Opt. Soc. Am.*, vol. 73, pp. 1165−1174.